Advanced Engineering Informatics 46 (2020) 101192

Contents lists available at ScienceDirect

Advanced Engineering Informatics

journal homepage: www.elsevier.com/locate/aei

A methodology of risk assessment, management, and coping actions for nuclear power plant (NPP) hit by high-explosive warheads

David Ornai [a], Sima Michal Elkabets [a], Yosef Kivity [a], Gabi Ben-Dor [b], Liran Chadad [a], Erez Gal [a], Barak Tavron [c], Erez Gilad [d], Robert Levy [a], Igal M. Shohet [a,e,*]

[a] Department of Structural Engineering, Faculty of Engineering Sciences, Ben-Gurion University of the Negev, P.O.B. 653, Beer-Sheva 8410501, Israel
[b] Department of Mechanical Engineering, Faculty of Engineering Sciences, Ben-Gurion University of the Negev, P.O.B. 653, Beer-Sheva 8410501, Israel
[c] Planning Development and Technology Division, Israel Electric Corporation, Haifa, Israel
[d] Unit of Nuclear Engineering, Faculty of Engineering Sciences, Ben-Gurion University of the Negev, P.O.B. 653, Beer-Sheva 8410501, Israel
[e] Dept. of Construction Engineering, ChaoYang University of Technology, Taichung, Taiwan, Republic of China

ARTICLE INFO

Keywords:
Blast
Fragmentation
Munition
Loss of Coolant Accident (LOCA)
Risk Management

ABSTRACT

A detailed Loss of Coolant Accident (LOCA) analysis in an AP1000 NPP was performed, followed by a definition of the vulnerability analysis principles, and analysis of blast loads and fragments impact created by a nearby explosion. The AP1000 NPP performs excellently to small-break LOCA due to in-structure shock, with the 10 CFR 50.46 Acceptance Criteria fully accomplished. Impulsive dynamic loads resulting from blast waves and fragments impact of GBU-28 (Guided Bomb Unit) were considered for a nearby explosion. We model the structure and the main reactor components using the MSC/Dytran code to obtain accurate internal acceleration levels at critical points. We account for the appropriate blast wave interaction with the soil and the soil interaction with the containment structure, rather than using empirical formulas. The model includes the shielding structure with its concrete base, the support structures for the reactor, the steam generators, and the pressurizer. The combined effect of bomb fragmentation and blast loading was also considered using a cylindrical fragmentation model and the blast model of Kingery-Bulmash, assuming a hemispherical charge. A comprehensive risk assessment methodology composed of four phases was developed. The methodology is comprised of: (I) System analysis, (II) Hazard analysis, (III) Damage assessment, and (IV) Risk analysis of the in-structure shock consequences. Using seismic fragility curves for analysis of the expected failure modes according to explosion events faced difficulties since no published data was found. Adjustments to these fragility curves were made using median acceleration limits on components designed to withstand airplane crash, together with standard deviations taken from the given earthquake fragility tables. The findings reveal that the probabilities of failure of the reactor coolant system components resulting from a GBU-28 nearby hit, namely the pressurizer, the cooling pumps, and valves are quite high (greater than $1 \cdot 10^{-4}$).

1. Introduction

Energy is one of the most important commodities for survival and continuous development of society. There is an increasing demand for low-carbon electricity, and renewable energy sources such as solar and wind energy are still in their infancy and, when used alone, are not realistic solutions to meet this demand. An alternative, safe, and low-carbon solution is to produce electricity by Nuclear Power Plant (NPP). The objective of the research is to develop a basic model for the assessment of the AP1000 NPP vulnerability to a threat scenario defined hereafter. The model is employed with the MSC/Dytran code [34] for simulating the effects of a bomb exploding nearby the shielding structure.

A similar study was carried out by [26] in their analysis of the vulnerability of NPP containment to blast loading. In their analysis, the internal structure was modeled as a lumped-mass stick, and other components were attached to the stick at discrete nodes. In the present analysis, however, the structural components were modeled using finite elements to yield more accurate acceleration levels at critical points.

Furthermore, we consider the appropriate blast wave interaction

* Corresponding author.
E-mail address: igals@bgu.ac.il (I.M. Shohet).

https://doi.org/10.1016/j.aei.2020.101192
Received 1 February 2020; Received in revised form 14 August 2020; Accepted 13 October 2020

with the soil and the soil interaction with the containment structure, rather than using empirical formulas, as was done in the Huang and Whittaker study [26]. The model includes the shielding structure with its concrete base, the support structures for the reactor, the steam generators, and the pressurizer. In future work, it is intended that the model will be progressively modified to include additional components of the power plant, such as the containment vessel. The primary objective is to obtain a first estimate of the acceleration levels induced by the hypothetical threat that would serve for analyzing various hypothetical LOCA scenarios. The present research focuses on the pressurizer valve, whose failure analyzed as a major accident root cause.

[9]developed an empirical numerical methodology for the assessment of the blast resistance and failure behavior of RC (reinforced concrete) and PSC (Pre-stressed Concrete) elements for nuclear containment vessels. The model yielded precise numerical assessment of the structural elements deflections. [58] developed a 3D FE numerical model for the prediction of the dynamic behavior of NRC (novel RC) slabs under contact blast loadings. The research findings indicated that the yield strength of the reinforcement is insensitive to the maximum displacement and stress states, and analytical formulae were developed to predict the maximum central deflection and blast resistance of slabs in terms of the explosive weight, standoff distance, and the slab thickness.

[57] developed nonlinear 3D FE models of RC slab, SSSC (Single-side- steel–concrete), and CSC (center steel–concrete) panels consisting steel plate, concrete infill, and shear connectors to assess the blast behaviors of these alternative structural elements for effective protection of NPP against contact blast loads. The SSSC and CSC slabs suffered larger damage than the RC slab. However, severe penetration damage with deteriorated load-bearing capacity was observed in the RC panel. The steel plate was found to have an important role in the SSSC and CSC slabs blast resistance. [29] introduced the implementation of Fiber Reinforced Concrete (FRC) for upgraded resistance of NPP against large commercial aircraft crash. The analysis results showed that the FRC displacement decreases by 43–67% while the impact-resistance increases by 40–82%, depending on the fiber type. [2] developed a methodology to obtain the response spectrum of a PWR building caused by underground blast. The reference scenario was defined as an explosion of 15 T of TNT at a distance of 2,000 m from the reactor building. The model included analytical and numerical modeling with explicit approach. It was found that the seismic response spectrums encase the blast response spectrum and that the horizontal velocity is below the limits established by the regulations. The structure was found to be safe under the given scenario.

A review of prior studies [25,26,37]reveals that NPP resistance to dynamic loads was analyzed based on analytical models considering blast and shock waves. The review indicates lack of integrated analysis of the blast and shock waves as well as the fragments and lack of a comprehensive risk analysis that integrates the vulnerability of all the critical components of the NPP.

1.1. Definition of generic scenario

The generic threat scenario was assumed as guided bomb unit, GBU-28 near-miss hits. Since the weapon is very accurate (circular error probability, CEP, of 20 ft), 50% of the launched munitions from an aircraft will hit within a circle of 20 ft (~6m) around the aiming point. In contrast, the others will hit at various distances with a normal distribution. It means that if the aiming point is the center of the AP1000 shielding structure, where the nuclear core is located, with a radius of about 22 m, then a direct internal hit is highly likely to happen.

Protecting against direct hits is not discussed in the present paper. The GBU-28 can penetrate about 6 m of concrete while the shielding structure has only 3 ft (~0.9 m) walls made of an internal steel plate, reinforced concrete wall, and an outer steel plate. Hence, the munition can penetrate the wall and explode afterward within the shielding structure. An existing unprotected AP1000 will be severely damaged in such a case. Given the presence of irradiated nuclear fuel in the reactor core, radioactive materials might leak to the atmosphere and the soil with long-term consequences. This scenario of internal hit should be carefully analyzed in a separate research.

This paper focuses on near-miss hit at 1 to 3 m from the exterior wall of the shielding structure at a center of gravity (c.g.) elevation of 2 and 4 m. The threat defined for the in-structure shock assumes a bare high-explosive charge as the load. The exact type of the explosive charge carried by the GBU-28 bomb is not known to us and is not publicly available. The charge mass is assumed to be 300 kg C-4 with an energy content of 5.62 MJ/kg, slightly larger than the 286 kg mass published for the GBU-28[48], to compensate for the more powerful explosive in the bomb. The physical model defined for the blast and fragment impact on the shielding structure took a cylindrical fragmentation case of the GBU-28 bomb. The research also provides an analytical–numerical method for evaluating the AP1000 NPP vulnerability to the above mentioned near-miss hits.

1.2. Definition of vulnerability principles

Three vulnerability principles of the GBU-28 external hit are defined as follows:

1. If the outer wall of the shielding structure is breached or perforated by the GBU-28 blast and fragments' impact, then the NPP should be shut down until it will be repaired. The risk might happen at contact hits up to standoff of approximately 1 m [43].
2. If the in-structure shock caused by the GBU-28 blast and fragments exceeds certain engineering systems and equipment shock tolerances, then internal failure is likely to happen. For example, a failure in the pressurizer or other safety systems may lead to a loss of coolant accident (LOCA) with a possible subsequent meltdown of the nuclear core and radioactive release to the atmosphere. The shock tolerances were taken from nuclear reactors' demands (Nuclear Energy Institute [36]). The relevant tables represent the median fragility limit of the NPP equipment exposed to an airplane crash, which has a longer duration than the munition hit and explosion. Nonetheless, it is much more suitable than seismic loading, which lasts much longer (seconds) with smaller accelerations (less than 1 g). Moreover, the characteristics of the seismic fragility curves of the AP1000 were adopted similar to MCEER-08–0019, 2008 [25].
3. Other vulnerable facilities within the NPP, such as the control room, should be investigated since their failure might cause LOCA or other NPP failures. In a previous study, a novel integrated blast resistance model (IBRM) was developed and demonstrated for a Scud B-100 missile explosion of 1000 kg of TNT exploding near the control room at various standoff distances [6]. There might be a failure of the internal engineering systems in case of an explosion at a standoff distance of 35 m and 60 m due to vertical and horizontal motions, respectively. At the same time, the exterior walls might cause spalling that might harm the occupants and the internal systems at a standoff distance of 20 m or less.

1.3. Modeling concepts for fragility quantification

[46] reviewed human-made incidents' effects in urban areas and emphasized the complexity of vulnerability and risk analyses in critical infrastructures. An integrated hierarchical modeling concept proposed to quantify the resilience of critical infrastructures combining structural and functional criteria. Major parameters of dynamic loads applied to structures by explosions such as times of arrival, peak pressures, durations, impulses, etc. are commonly assessed based on large empirical data. These parameters presented in charts for a range of charge weights and standoff distances [44,28,45,12]. Oliveira et al. [37] determined the blast pressures of a 100,000 lb TNT hemispherical charge by finite element model that simulates the shock wave propagation considering

the topographical features of the site and the main structures of the NPP.

A simplistic method of evaluating components' fragility is to convert the impulse of the reflected overpressure into kinetic energy and compare it with the strain energy of the structure to assess the expected damage [7,4]. At this stage (after hazard analysis, blast load calculation, and fragility evaluation of critical components analysis), *iso*-damage contour circles around a given explosive charge can be introduced, where the damage lines correspond to the vulnerability analysis. These contours can be used to distinguish between safe or unsafe regions for different types of engineering systems and components depend upon their vulnerability. Safe regions for a given explosion are presented in contours; moreover, using these contours, a critical zone can be located. An example of a critical zone can be a location that, if an explosion was located in, both a critical component and its backup component would be damaged simultaneously.

Nevertheless, this method does not consider the reduction in the blast overpressure due to obstacles in the blast wave propagation path. To evaluate a reinforced concrete containment shell exposed to the blast, [39] developed a finite element software which applies non-linearity phenomena such as pressure sensitivity in three-dimensional loading condition, strain-rate sensitivity, and cracking. A demonstrative containment shell subjected to surface blast loading of 20 ton TNT at a distance of 100 m. and to a 0.25 ton and 0.5 ton TNT at a distance of 20 m was analyzed. The peak shell deflection was 58.8 mm for the close-range charge of 0.5 ton and 91.8 mm for the long-range charge. The shell was capable of withstanding the blast loads, though little damage was detected.

1.4. Structural retrofit methods against explosions

The current worldwide passive structural retrofit methods against explosions can be categorized into three main types: strengthening methods, shielding methods, and control hazardous debris methods [32]. Strengthening methods enlarge element dimensions and increase its resistance capacities, including connections strengthening, element sizes enlargement, and span reduction. An advanced strengthening solution uses high strength fiber mats or strips, including carbon, kevlar, glass, or aramid fibers embedded in a polymer matrix such as an epoxy resin. They are attached to existing structural components while providing enhanced shear and flexural capacities as well as confinement. They allow the structural component to deform extensively while maintaining or even increasing its load-bearing capacity [3,17,41,22,14,24].

Blast shielding methods prevent structural components from being fully loaded by adding a sacrificial cladding layer to structural components exposed to the blast. It is designed to have high absorption energy capacity, so reduced impulse is transferred to the structure, and it can be applied locally, e.g., by the construction of a new wall that protects a vulnerable component or a branch of the building. Additional alternatives are protecting the vulnerable component by building of a new protective RC (Reinforced Concrete) or steel structure over the existing building [1,35,42,56,21,38,47]. Control of hazardous debris methods stop or deflect the failed exterior protective layer away from internal critical areas by using catch systems or internal protective walls and panels [18].

An active control approach is also attracting considerable attention. Under this approach, one can find solutions based on sensors and actuators that will activate a blast-mitigating device using explosives when an explosion is identified [33]. Passive concepts have the important advantage of operating by the striking blast wave independently from energy source and complicated systems. It is hard to guarantee that a sensor or an actuator, which is not in use for an extended period, will work properly or will not be damaged during the impact event. Active systems also have false alarm problems as part of their performance. The disadvantage of the afore-mentioned passive concepts is that they consume additional protective material to achieve efficient reduction. Some of the active and passive approaches can protect against a single blast event only.

Solutions using passive control devices for seismic events are widespread [10]. These devices, such as viscous and friction dampers, can be added to an existing structure without functional interruption and drastic changes in the geometry and weight of the structure. The obstacle of using them for blast mitigation is because the devices should respond during a very short time, the first quarter of the natural response period of the structure. This period is very short in the case of fully constrained structures. One can find limited use of those devices for framed structures exposed to blast events [8].

2. Accident scenarios

2.1. Introduction

In what follows, we describe the LOCA accident scenario in an AP1000 NPP. This accident scenario represents a class of severe accidents that could result in severe outcomes such as core meltdown and significant release of radioactive fission products to the atmosphere. The relevant failure scenarios reviewed are taken from the Westinghouse AP1000 DCD Rev. 19 submitted to the NRC [51].

2.2. A decrease in reactor coolant inventory

The following events that may lead to a reduction in reactor coolant inventory [51]:

- A rupture or a breach in a steam generator's pipe.
- A rupture or a breach in the outer boundary surfaces of the primary or secondary pressurized coolant system;
- An unintentional release of a safety piston in the pressurizer or accidental activation of the automatic depressurization system (ADS);
- A variety of hypothesized ruptures or breaches of pipes within the reactor pressurized coolant boundary resulting in LOCA.

The applicable accidents in this category have been analyzed. It has been determined that the most severe radiological consequences result from the major LOCA described in the following paragraph.

2.3. Loss-of-Coolant accidents (LOCA)

When the pressurized coolant pipes in the reactor are punctured, a LOCA can be triggered. Usually, a pipe break is considered significant if the fracture is characterized by a cross-section of one square foot (or larger). The probability of such an incident is so small that it is not supposed to happen within the 60–80 years of the NPP operation period. Hence, it is a conservative hypothesized design basis accident, categorized as a Condition IV event (a limiting fault).

A small rupture is characterized by a cross-section smaller than one square foot. However, the loss of coolant rate is large enough so that the pressure and coolant amount of the pressurizer cannot be maintained by the compensation of the recharging systems. The probability of such an incident is small, but it may still happen within the operation period of the NPP. Hence, it is a hypothesized design basis fault, categorized as a Condition III event.

The NRC LOCA acceptance criteria are [50]:

- The fuel cladding temperature will be less than 2200°F during the entire simulated scenario.
- The reduction in cladding width, at any point, due to oxidation, will be less than 17% of the initial width.
- The production of hydrogen by steam-cladding oxidation will be limited to 1% of the theoretical maximal amount.

- Changes in core geometry will not damage the cooling capacity of the fuel.
- The fuel and cladding temperatures remain low indefinitely, by accounting for the removal of residual decay heat.

Furthermore, in the AP1000 Final Safety Evaluation Report [49], the unintentional opening of a pressurizer safety valve is among the events that may lead to a decrease in reactor coolant inventory (LOCA). This event leads to a rapid depressurization of the reactor coolant system, followed by a decline in power via the moderator temperature reactivity feedback. The average coolant temperature gradually decreases, and the pressurizer level increases until the reactor SCRAM (Safety control rod axe man). This event is categorized as a fault of moderate frequency.

The accidental opening of a pressurizer safety valve can only be hypothesized due to a mechanical failure. This is the reason this event was chosen to demonstrate the methodology developed in this research. This mechanical failure of the pressurizer safety valve is hypothesized to be triggered by the GBU-28 near-miss hit, which is a highly reasonable assumption.

Generally, the above criteria are intended to allow a substantial operation margin in emergency core cooling system performance following a LOCA. For the AP1000, the small breaks scenarios are characterized by larger margin than large breaks.

3. The vulnerability of the shielding structure wall

The shielding structure cylindrical wall that surrounds the containment vessel and the nuclear reactor in it is 44 m in diameter and 64 m in height. The wall section has two mild steel layers (internal and external), each layer thickness equals 19 mm, and the concrete fill is 0.88 m wide. The concrete nominal compression strength equals 6000 psi (41.4 MPa). Impulsive loads on a structure arise due to blast and fragments impact created by a nearby explosion of cased munition (in this research GBU-28). The near-miss hit is of a vertical GBU-28 a few meters parallel to the wall is shown in Fig. 1. Both the blast and fragment loading were calculated according to the assumed data of GBU-28 given in Table 1.

The equivalent bare charge of the real cased munition is calculated according to Fano's formula given by Crowley [11]. Then the blast loading is calculated according to Swisdak [45] as an equivalent hemispherical charge while applying a 20% factor of safety due to the many uncertainties [12]. The Drake et al. [13] fragment cylindrical model [13] is used for the addition of the fragments loading, while the bomb is assumed as uniform cylindrical shaped, and the fragments are equally dispersed perpendicularly to the munition axis. The mutual blast and fragments loading at 1 m and 3 m standoff distances from the wall were calculated, as shown in Fig. 2.

A dynamic analysis of the shielding structure exposed to blast and fragments of the near-miss explosions was carried out for 1 m and 3 m standoff distances. It was based on Abaqus CAE 2017 finite elements software using 0.5 m × 0.5 m shell elements with 0.1 ms time steps (Fig. 1). Materials data are as follows: Concrete Young Modulus Ec = 30 GPa, Concrete compression strength was rounded to f`c = 40 MPa, Steel Young Modulus Ec = 210 GPa, and Steel compression strength fsk = 400 MPa. The concrete wall thickness was rounded to 0.9 m, and the thickness of each of the steel layers was rounded to 0.02 m.

The dynamic loading on the analyzed target shown in Fig. 2 included the combined impulse of blast and fragments at 1 m and 3 m standoff distances (Fig. 3). The analysis result shown in Fig. 4 for 1 m standoff distance defines strength failure of the shielding wall in two areas of 0.25 m^2 since the stresses (in red) equal to 4.0E + 08 Pa (400 MPa) are higher than the composite wall resistance capacity. In comparison, at 3 m no failure is expected.

Two empirical approaches were employed for an assumed equivalent reinforced concrete wall of 1.8 m wide to get an approximation of the steel–concrete-steel resistance to contact and near-miss explosion. The maximal standoff distance between the GBU-28 axis and the wall face, R (m), in which breaching will occur is 0.48 m and 0.82 m, according to [55] and [13], respectively. The wall is supposed to be breached or perforated by the GBU-28 blast only from contact explosion up to 0.6 m ± 0.12 m. It means that the fragments are captured in the concrete between the two steel layers, and breaching or penetration through are not expected.

Based on empirical data for various ranges up to contact, the UFC 3–340-02[12] determines an increased reinforced concrete wall thickness required to resist combined blast and fragments in comparison with blast only. Our numerical results that agglomerated fragment and air blast loads estimate a wall failure up to 1 m standoff. It is a little bit greater than 0.6 m ± 0.12 m based on empirical data, assuming an equivalent reinforced concrete wall of 1.8 m wide [13,23,55]. Hence this approach is adequate, and the results are validated.

4. AP1000 In-structure shock response to blast loading

The purpose of the analysis is to build a basic model for the AP1000 nuclear power plant that would enable the assessment of the plant vulnerability to the given threat scenarios. The basic model is employed with the MSC/Dytran code for simulating the effects of a bomb exploding nearby the shielding structure.

4.1. Case setup

The detonation of the bomb creates two effects: A blast wave, which interacts with the building creating a **global** structural response, and kinetic energy fragments that hit the wall of the building, creating **localized** damage. We consider here only the blast wave effect of the bomb. The localized effect of the fragments will be considered separately. Furthermore, to be on the safe side, the entire energy content of the explosive will be taken for creating the blast, even though part of the explosive energy is spent in accelerating the casing fragments [11,27]. The shielding structure cross-section was modeled as a sandwich of concrete and two thin steel liners. The concrete was modeled as a "solid"[1] with a thickness of 0.9 m and the steel liners were modeled as "thin shells"[2] with a thickness of 19 mm. The structure was loaded at its side, 3 m away from the shielding wall, and 4 m above ground level, with the ground modeled as an elastic medium. The soil parameters were defined as follows: Soil density ρ = 1920 kg/m^3, Young Modulus E = 51.7 MPa, Poisson ratio equals 0.45.

4.2. Finite element model

The model of the structural components defined as finite element structures to obtain accurate acceleration levels at the NPP critical points. Furthermore, the appropriate blast wave interaction with the soil and the soil interaction with the containment structure were considered, rather than use empirical formulas, as was done in previous studies [26]. The model includes the shielding structure with its concrete base, the support structures for the reactor, the steam generators, and the pressurizer. The shielding structure is basically a cylinder closed by two end caps. The shape of the end bottom cap is circular, and the shape of the top cap is conical. It supports the cooling water pool situated on top of it. The concrete and steel parameters used for the numerical analyses were as follows: concrete compression strength f`c = 40 MPa, steel Young modulus Ec = 210 GPa, and the steel compression and tension strengths fs = 400 MPa.

We employ a symmetrical half of the structure, assuming

[1] This term is taken from the finite element usage. It refers to a full three dimensional body.

[2] This term is taken from the finite element usage. It refers to a thin body described by a surface, whereby the thickness appears only as a parameter of the model.

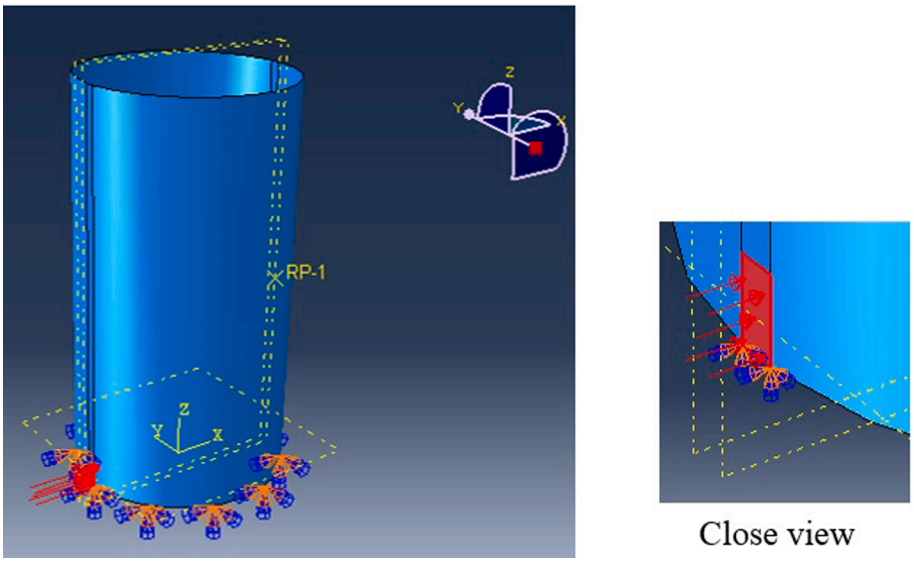

Fig. 1. Modeling the shielding wall using 0.5 m × 0.5 m shell elements.

Table 1
Assumed data of GBU-28.

Characteristic	Value
External diameter [mm]	388
Internal diameter [mm]	203
Casing thickness [mm]	93
Explosive density [kg/m^3]	1,720
Charge mass [kg TNT]	300
Bomb length [m]	4.04
Casing density [kg/m^3]	7,850
Casing mass [kg]	2,696

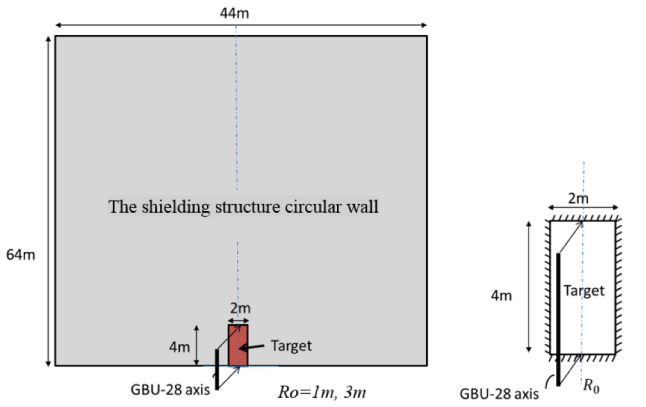

Fig. 2. The analyzed target.

symmetrical loading with respect to a vertical plane passing through the axis of symmetry. The cylinder diameter was taken as 44 m. and its height as 64 m. These dimensions and others were extracted from the Westinghouse AP1000 design control document [52] and a geometrical model shown in Figs. 5 and 6 were assembled. For the support structures of the reactor and steam generators, we take an approximate symmetrical half. The dynamic structural behavior was analyzed using time histories of the dynamic response for the pressurizer top (denoted by PRZ in Fig. 7). This point was selected as the pressurizer safety nozzle was found to be most critical for the pressurizer continuous performance.

4.3. Explosive charge

The small size of the explosive charge (relative to the typical dimensions of the structure) makes it inefficient to represent it directly in the mesh of the flow field. Therefore, we employ a pre-calculation for creating the blast wave flow field. First, the blast wave can develop into its immediate close vicinity, and then this flow field is remapped into the general mesh. Fig. 8 shows the initial state of the cylindrical charge in a two dimensional axially symmetric mesh, with the dimensions of 3 m × 6 m. The cylinder center is located at mid-height of the mesh. Figs. 9–11 show the development of the flow field in terms of velocity and density maps in three equal time intervals of 0.2 ms.

Since the point of initiation within the charge was not specified, a simultaneous initiation was assumed for simplicity, according to the CVD[3] (Constant Volume Detonation) model.

4.4. Results

The interaction between the blast wave and the structure was carried out using a special coupling algorithm between the pressure field created by the explosion and the finite elements representing the structure. The blast wave propagates in a mesh, which is fixed in space, an Eulerian mesh, sometimes referred to as a "finite volume" mesh. When the local flow field around the charge has been calculated (in the current example, the flow field at 0.6 ms), it can be remapped into a specified location in the Eulerian mesh where the structure is embedded. Fig. 12 shows the initial density map for the symmetrical half of the model. From this point on, the code calculates the evolution in time of the blast wave and its interaction with the structure. Figs. 13–16 show pressure and displacement maps for selected times. The displacements are of the order of 10 mm, and the pressure in the blast wave ranges from about 10 bar in the air at 5 ms to 3 bar in the soil at 80 ms. The maps at 40 ms and 80 ms show that the blast wavefront is progressing down into the soil and that the peak pressure is actually in the soil beneath the shielding structure.

Of the displacement components, the in-plane horizontal one was found to be the largest (Fig. 17). This is to be expected since the blast wave excitation is coming from this direction. There is a high-frequency component, which comes from the pressurizer natural frequency, and a

[3] According to this widely accepted model the entire energy of the explosive is released instantaneously.

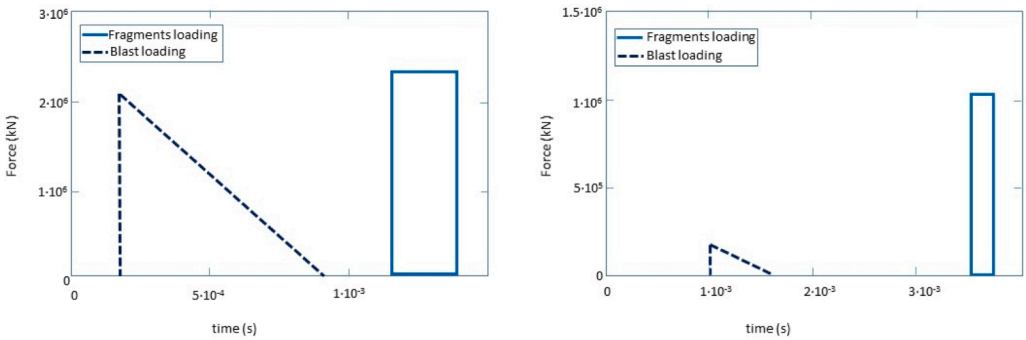

a. 1 m standoff b. 3 m standoff

Fig. 3. Blast and fragment loading versus time at 1 and 3 m standoff distances from the shielding structure wall.

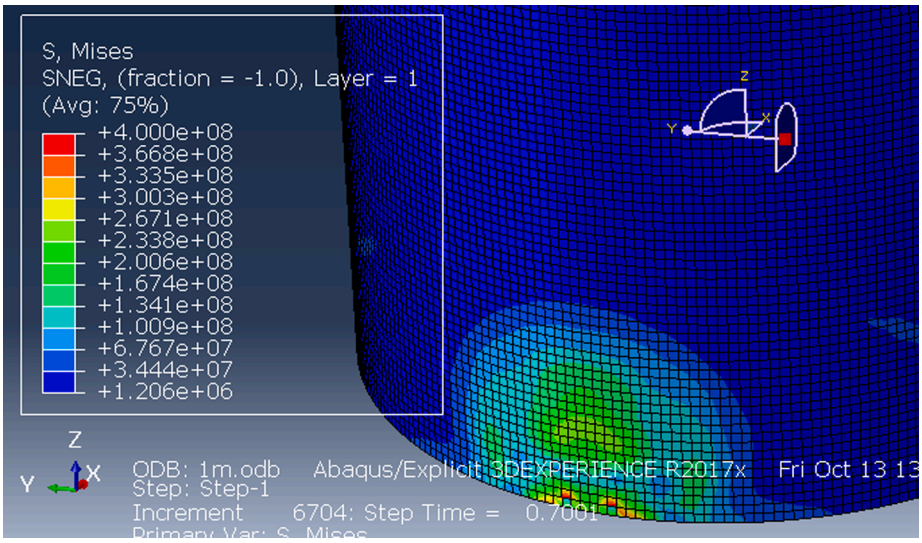

Fig. 4. Maximum Mises stresses at a standoff distance of 1 m.

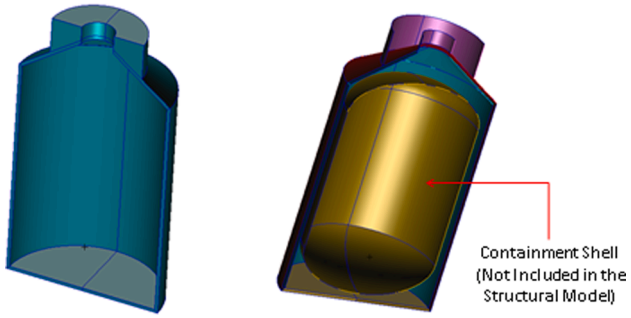

Fig. 5. Geometry of a symmetrical half of the shielding structure.

much slower frequency coming from the response of the heavy concrete base. The latter is evident in the in-plane horizontal component. The velocity components are of the order of 0.15 m/s, with occasional peaks of the horizontal in-plane component attaining 0.25 m/s (Fig. 18). The peak acceleration components are of the order of 10 g, with occasional overshoots to ~12 g (Fig. 19).

5. Risk assessment

Seismic fragility curves are implemented to analyze structural seismic failure probability. Fragility is expressed by a probability of

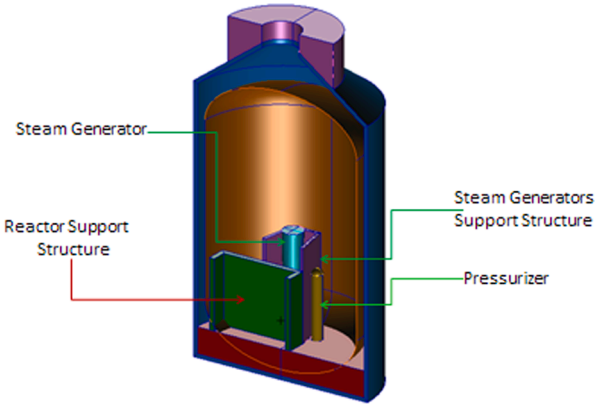

Fig. 6. The shielding structure with the support structures, the containment shell, the steam generator and the pressurizer.

failure as a function of the seismic ground motion intensity parameter inducing different damage states. Alternative seismic ground motion intensity parameters, such as peak ground acceleration, peak ground velocity, peak ground displacement, and pseudo-spectral acceleration, are used for different types of structures and components such as above-ground structures, underground pipes, etc. The lognormal fragility curve was defined by the median structural ground acceleration capacity and

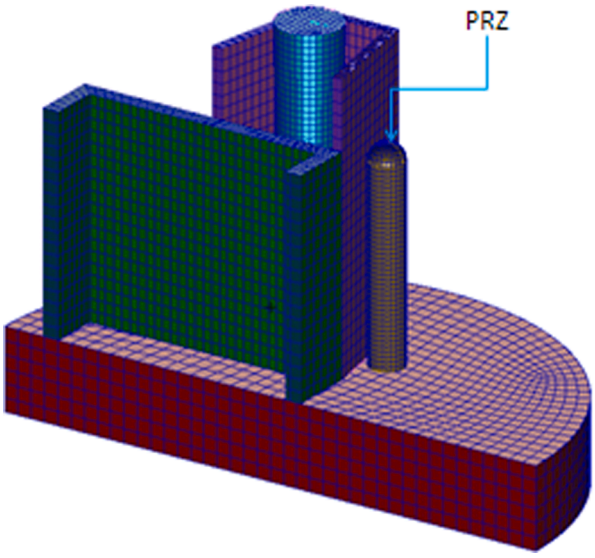

Fig. 7. Gauge location for monitoring the top of the pressurizer (safety valve).

two logarithmic standard deviations, as expressed in Eq. (1) [31]:

$$f = \Phi\left[\frac{\ln(a) - \ln(A_M) + \beta u \Phi^{-1}(Q)}{\beta r}\right] = \Phi\left[\frac{\ln\left(\frac{a}{A_M}\right) + \beta_u \Phi^{-1}(Q)}{\beta_r}\right] \quad (1)$$

Here, f denotes the cumulative density of the fragility function, Φ denotes the standard Gaussian cumulative distribution, and Φ^{-1} denotes the inverse Gaussian cumulative distribution function. A_M denotes the median ground acceleration capacity of the structure, a denotes the intensity measure, and Q the non-exceeding probability level. Two logarithmic standard deviations represent two complimentary composites of uncertainty. The first is a deviation of the inherent randomness of the natural phenomenon, β_r, which cannot be reduced by improving knowledge and modeling. For the seismic fragility curve, this uncertainty is caused by the randomness of ground motion parameters and by the dynamic response parameters of the structure. This uncertainty defines the incline of the fragility curve. The second component of the uncertainty, β_u, expresses the lack of complete knowledge about material properties, modeling assumptions, and so on. β_u expresses the uncertainty of the median.

A best estimate fragility curve may be defined using a composite of the randomness and uncertainty variability. The composite variability β_c is defined as:

$$\beta_c = (\beta_r^2 + \beta_u^2)^{0.5} \quad (2)$$

According to the AP1000 Design Control Document [51], a probabilistic fragility analysis was carried out for components such as steam generators support, reactor pressure vessel supports, pressurizer supports, and the containment vessel. This document defines the **HCLPF**, the High Confidence Low Probability of Failures as the peak ground acceleration level that reflects a 95% confidence (probability) of not exceeding a 5% probability of failure (approximately 95% confidence that the probability of failure is less than about 5%). In other words, the HCLPF is the ground acceleration level for which we have a low probability of failure in high confidence for a particular component.

In the AP1000 Design Control Document,

$$\text{HCLPF} = \text{MedianCapacity} e^{[-2.3 \cdot \beta_c]} \quad (3)$$

The median seismic capacity is related to the mean seismic capacity by the following expression:

$$\text{Mediancapacity} = \text{MeanCapacity} e^{-\left(\frac{\beta_c^2}{2}\right)} \quad (4)$$

The mean peak seismic ground capacity, AM, is related to the stress and strength design margin factors by the following expression:

$$\text{AM} = \left(\prod_i [X_i]\right) A_o \quad (5)$$

$$\beta_c = \sqrt{\sum_i (\beta_c)_i^2} \quad (6)$$

where,

AM – Mean peak seismic ground capacity

X_i- i^{th} design margin factor

A_o- Nominal seismic peak ground capacity

β_c- The composite standard deviation associated with each of the margin factors.

The differences between these references in defining the HCLPF level are found in the fact that in the AP1000 design control document assumption of $\beta_r = \beta_u$. Fig. 20 shows fragility curves at different confidence levels, such as 5%, 50%, and 95%. The 95% confidence curve means that the analyst has 95% confidence that the "true" fragility curve lies to the right of (higher than) the 95% curve shown. The mean fragility curve is shown in Fig. 20 and is the average of all possible fragility curves.

Solution of the flow field is accomplished in 2D taking advantage of the inherent symmetry of the problem. For simplicity, an instantaneous initiation is assumed, but specified point (or points) of initiation can be defined.

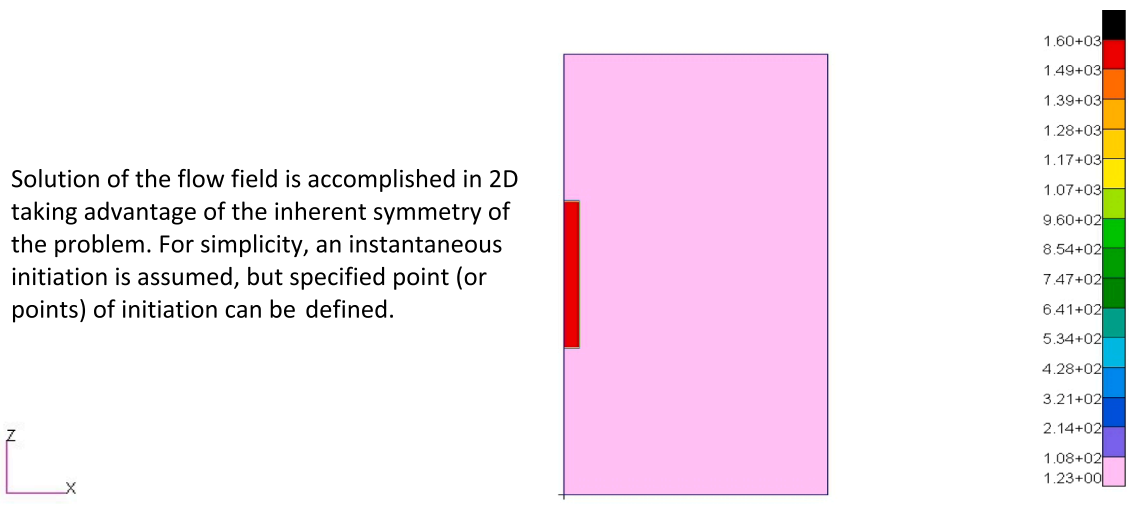

Fig. 8. Density map showing the initial state of the charge.

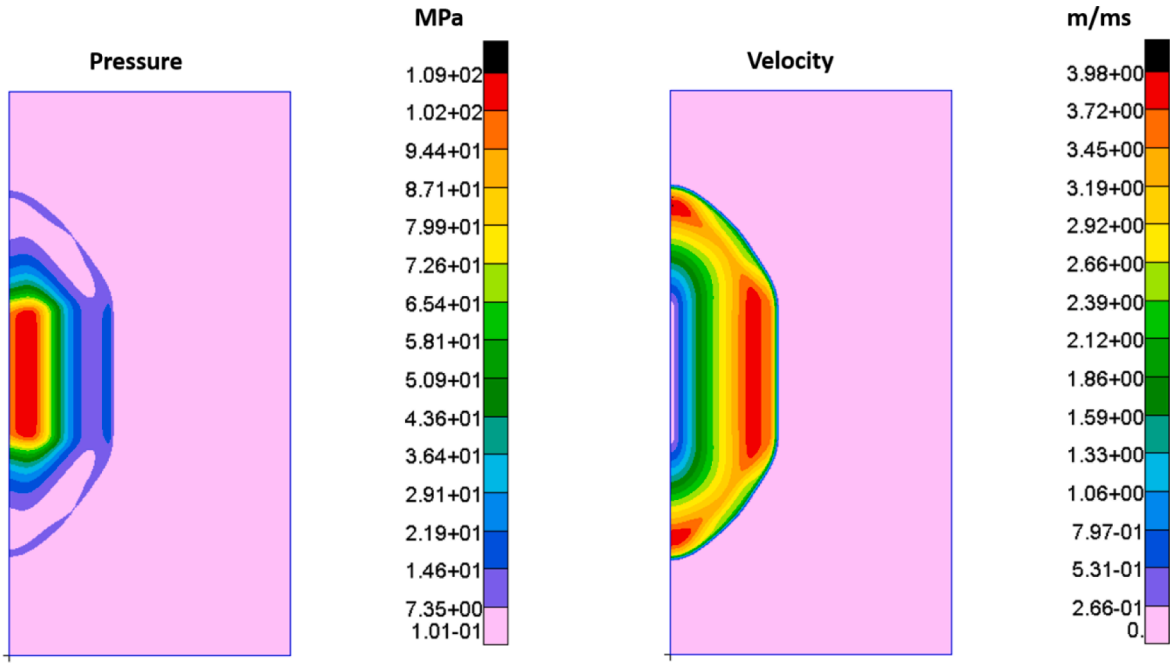

Fig. 9. Blast wave flow field at t = 0.2 ms after detonation.

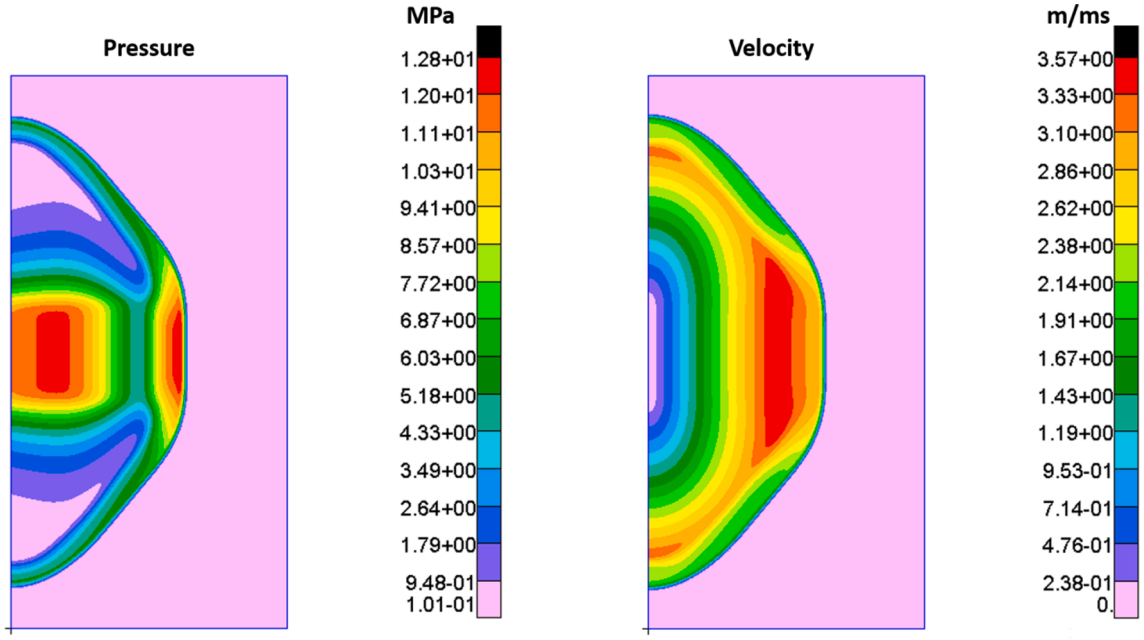

Fig. 10. Blast wave flow field at t = 0.4 ms after detonation.

For example, the fragility curve and the HCLPF factor will be as follows:

$$\text{HCLPF} = \text{MedianCapacity}\cdot e^{[-2.3\cdot\beta_c]} = 2.2\cdot e^{[-2.3\cdot 0.51]} = 0.68PGA\cdot \quad (7)$$

This means that for peak ground acceleration (PGA) of 0.68 g, there is a 5% failure in the confidence level of 95%.

Fig. 21 describes the cumulative distribution function that gives the probability of failure conditional on the demand (PGA). This figure was obtained using Eq. (3) with a median PGA of 0.68 g and $\beta_c = 0.51$, as derived from Eq.. It was computed for 200 simulated data points.

5.1. Probabilistic risk assessment model

The Probabilistic Risk Assessment Model for the AP1000 NPP to determine the risks due to GBU-28 explosion is composed of four major phases, as depicted in Fig. 22 and described hereinafter:

- *Phase 1*: Systems Analysis - this phase includes two layers: Organization layer - describes the main missions of the NPP, the regulatory, the strategic, the operational, and the human facets. The physical layer describes the assets systems and components, the functional relationships between them, their importance to the mission performance, and their vulnerability to an undesired extreme event. This layer considers the physical infrastructures and services, which

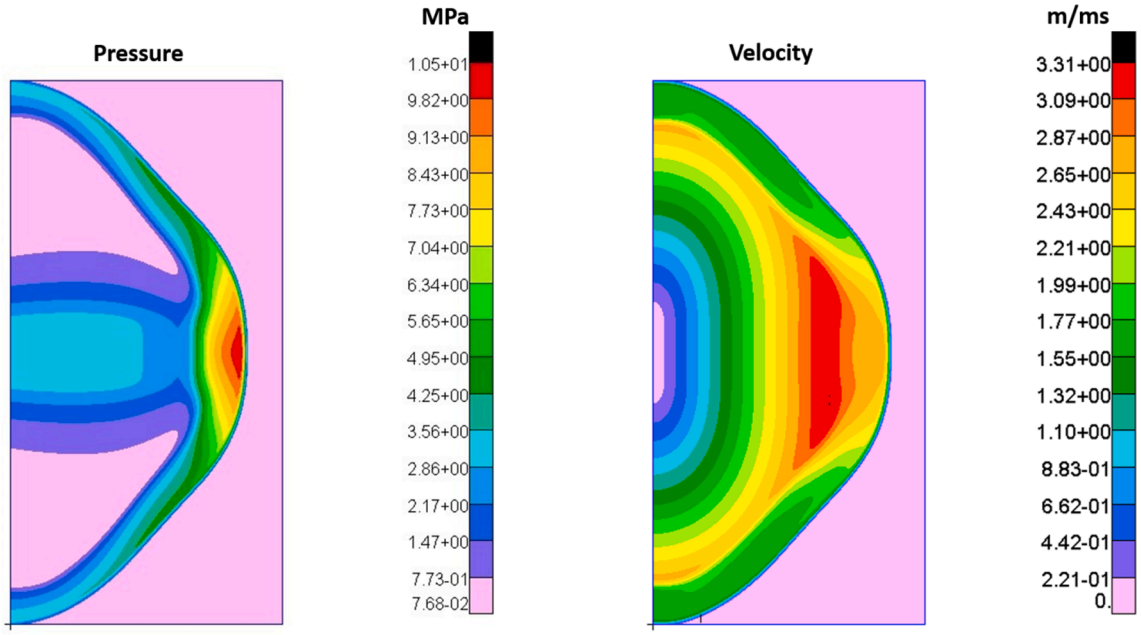

Fig. 11. Blast wave flow field at t = 0.6 ms after detonation.

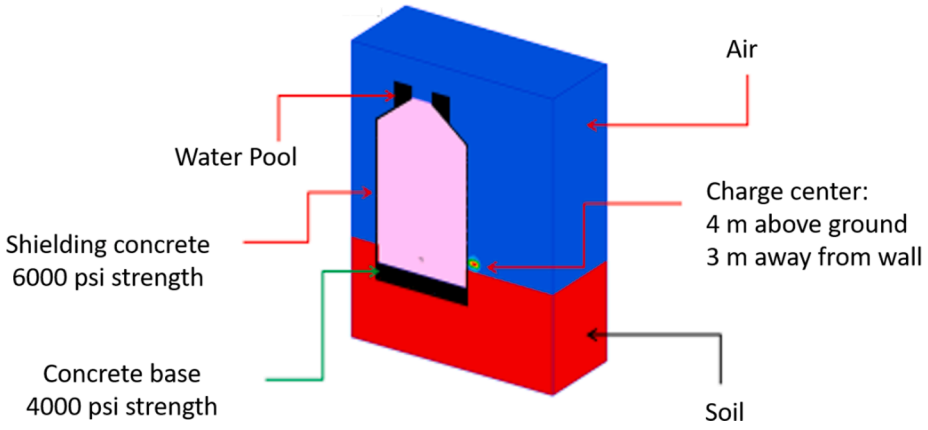

Fig. 12. Initial state of the problem – side hit with soil effect.

could be relevant to the NPP probabilistic risk analysis such as land, road access, buildings, water, power infrastructure, etc.

The system analysis, which was based on the AP1000 Design Control Document [51], indicated five critical systems for the LOCA scenario, including the piping system, the reactor vessel, the steam generators, the pressurizer, and the main coolant pumps. These critical systems are further considered in the following phases, as demonstrated in Fig. 23.

- *Phase 2*: Hazards Analysis - this phase includes two steps: 1) definition of the threat scenario, 2) definition of the failure event (such as LOCA). The obtained result of steps 1 and 2 is a framework for identification of the critical assets requiring protection and prioritization of the NPP from Core Melt Down situation by using: Failure Mode and Effects Analysis [19,20], Failure Mode, Effects and Criticality Analysis [16], Event Trees [15,30,40], and Fault Tree Analysis methods [44,5,53,54].

The results of the first two steps lead to the failure modes of the critical systems identified in phase 1, i.e., a pipe rupture of the reactor main coolant system (hot leg and cold leg pipes), rupture of the pressurizer safety relief nozzle, damage to the reactor vessel and steam generators, and malfunction of the main circulation coolant pumps.

- *Phase 3*: Damage Assessment - assessment of the level of damage state according to 5-point damage state rating scale. In this stage, the conversion of the data gathered from the explosion simulations to seismic values is carried out. That will be the foundation of the ability to use fragility curves (with modification and adaptation to explosion events) and to compare these values to the design values, as found in the manufacturer design documents submitted to the U.S. NRC.
- *Phase 4*: Risk Analysis - this phase includes the evaluation of risks using Eq. (8) and consequences analysis.

$$R = P \cdot C \tag{8}$$

where, R is the Risk, P is the Probability of the undesired event, and C is the Consequences. Common criteria or units of consequence include casualties, injuries, direct and indirect economic losses for the owner of the facility, direct and indirect economic losses for customers, loss of operation or production of the NPP (downtime), loss of public confidence, loss of assets and property, environmental impact, etc. The

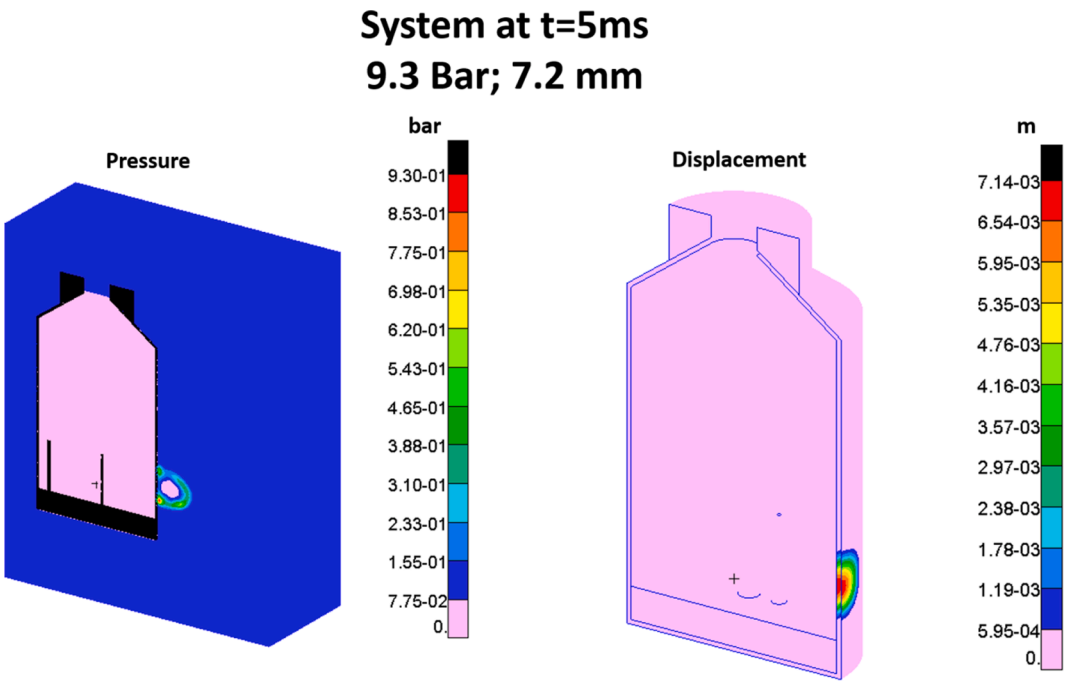

Fig. 13. Pressure and displacement maps at t = 5 ms.

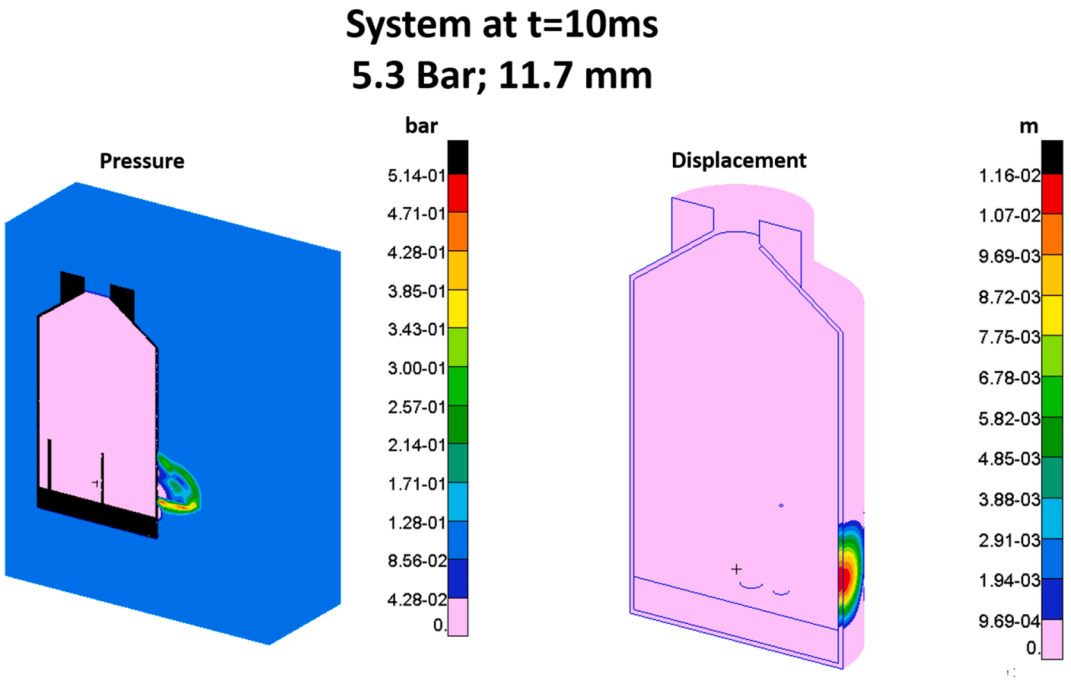

Fig. 14. Pressure and displacement maps at t = 10 ms.

reactor cooling systems and their components were reviewed. Fig. 22 describes the fault tree for this system failure.

According to the Fault-Tree presented in Fig. 21, the probability of RCS failure (RCS_F) is:

$$P(RCS_F) = 1 - \{[1 - P(f1)] \cdot [1 - P(f2)] \cdot [1 - P(f3)] \cdot [1 - P(f4)] \cdot [1 - P(f5)]\} \quad (9)$$

Where, RCS_F – Reactor Coolant System probability failure, P(*f1*) – Probability of failure in pipe systems, P(*f2*) – Probability of failure in reactor vessel, P(*f3*) – Probability of failure in steam generators, P(*f4*) – Probability of failure in pressurizer , and P(*f5*) – Probability of failure in coolant pumps. The lower and upper bounds of the probability of the basic events as well as of the RCS_F top event were derived and shown in Table 2.

The analysis results presented in Table 2 assumes that the median fragility limit of all components in the systems analysis is equal to 27 g, based on the lower limit in Table 3 from NEI 07–13 (Revision 8P) [36]. This is a conservative approach that assumed the lower bound of fragilities to all the RCS components. The mean probabilities of failures of the critical components at the primary coolant cycle are found to up to $5 \cdot 10^{-2}$ and the subsequent mean probability of RCS_F event under the occurrence of the reference scenario is $8 \cdot 10^{-2}$. This probability of

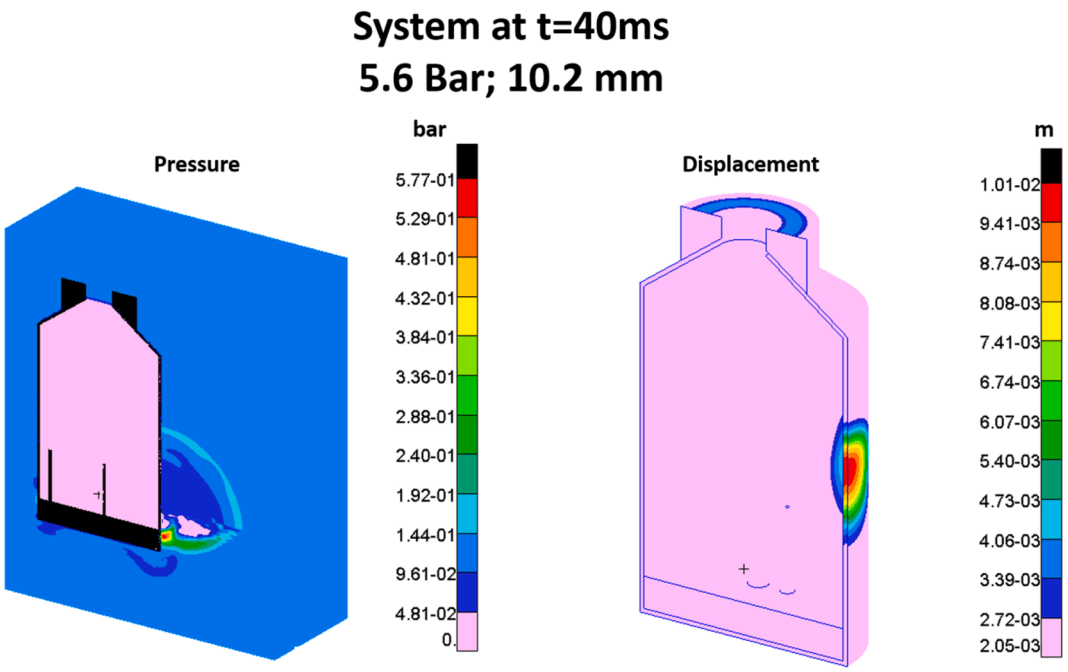

Fig. 15. Pressure and displacement maps at t = 40 ms.

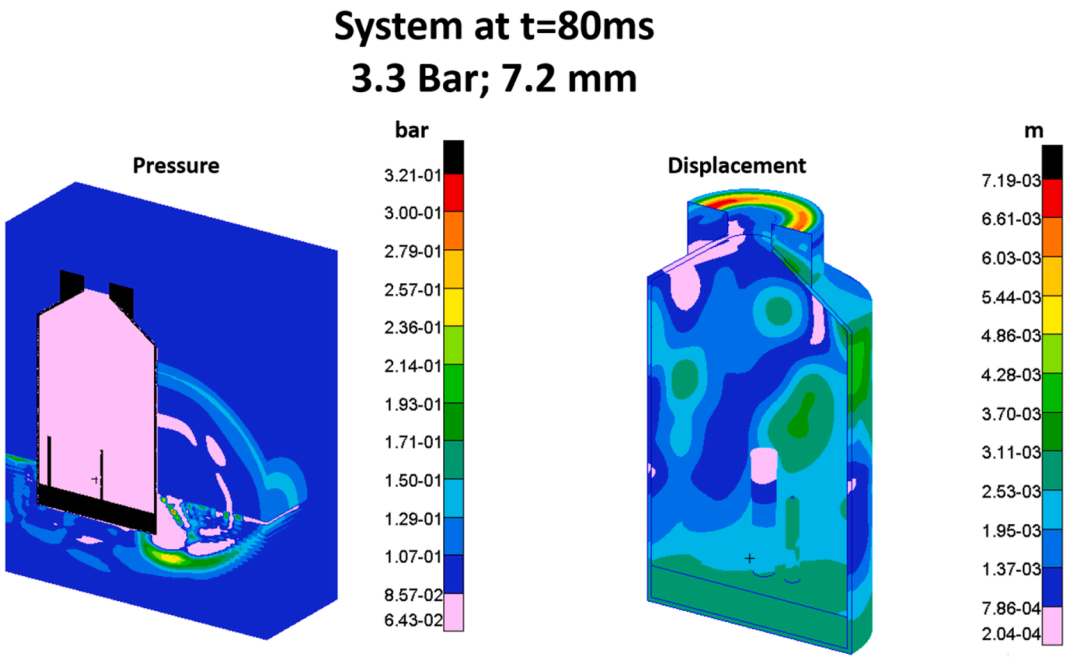

Fig. 16. Pressure and displacement maps at t = 80 ms.

failure considering the occurrence of the threat scenario event.

Table 3 presents the lower and upper bounds of the probability of the basic events as well as of the RCSF top event. Here, median capacity limits were best matched to the equipment functions as appears in Table 3 from NEI 07–13 (Revision 8P). The mean probabilities of failures of the critical components at the primary coolant cycle are found to be up to 5·10-2 and the subsequent mean probability of RCSF event under the occurrence of the reference scenario is 8·10-2. This probability of failure is for the occurrence of the threat scenario event.

Considering the results presented in Tables 2 and 3, it is evident that the scenario of a rupture or a breakdown in the reactor coolant primary pipes system is the most vulnerable component among all other critical components of the AP1000 NPP coolant system. Moreover, the RCSF value is dominated by the mean probability of failure of the pipes system, in both the conservative and the moderate approaches. Furthermore, while the mean probability of failure of the pipes system is largely insensitive to the analysis approach (moderate vs. conservative), the mean probability of failure of the other components is dramatically smaller in the moderate approach with respect to the conservative one. This is due to the large variability in the median capacity used in each approach.

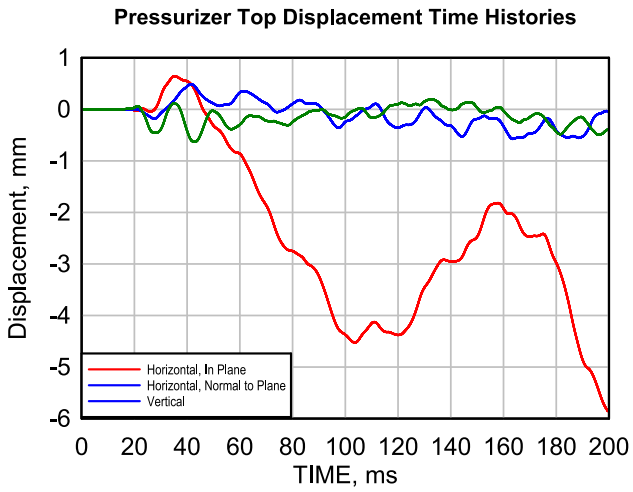

Fig. 17. Time histories of the pressurizer top displacement components.

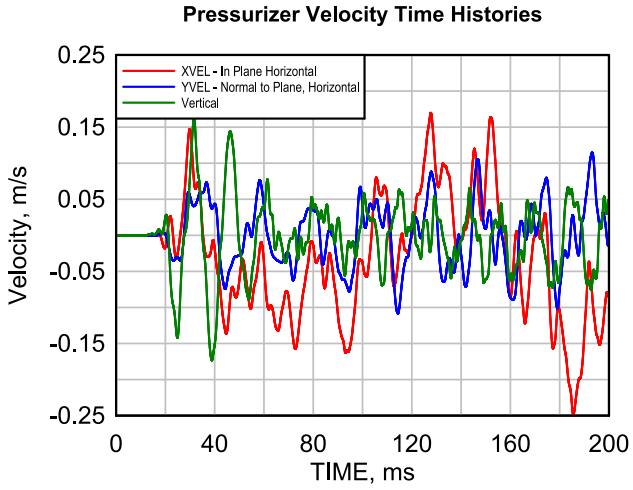

Fig. 18. Time histories of the pressurizer top velocity components.

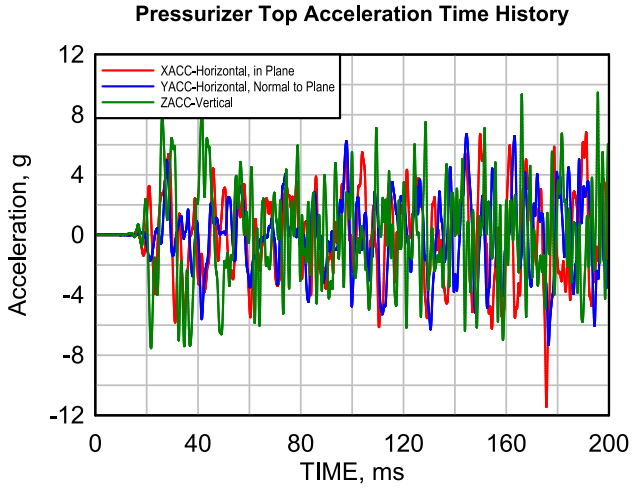

Fig. 19. Time histories of the pressurizer top acceleration components.

5.2. Damage assessment

To evaluate the probability of failure of the critical components described in Fig. 23, we use fragility curves. Fragility curves of the

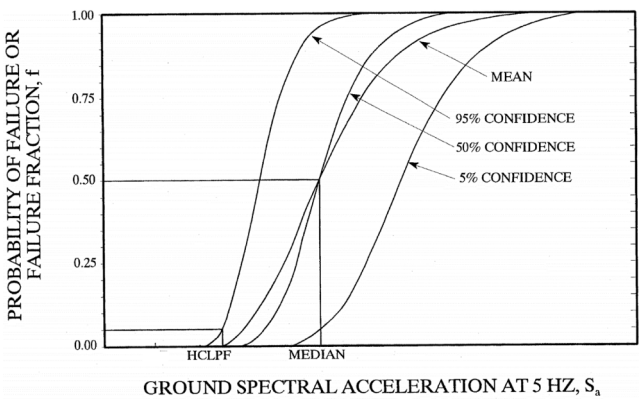

Fig. 20. illustration of fragility curves.

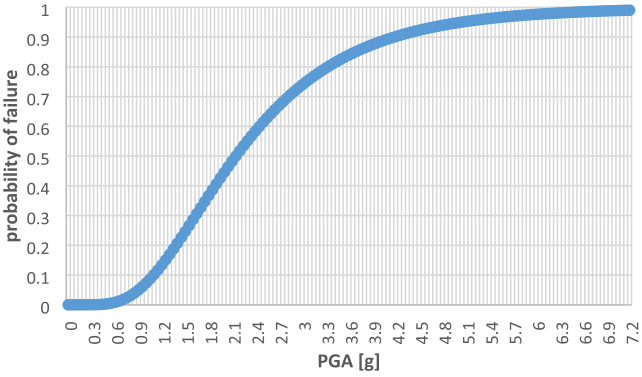

Fig. 21. Example of fragility curve derived from the AP1000 design control document analyses data for reactor coolant pumps.

AP1000 critical components for conventional explosions were developed using two assumptions. The median fragility was adopted from (Nuclear Energy [36] NEI 07–13 (Revision 8P). The relevant parameters represent the median fragility limit of the NPP equipment exposed to aircraft impact. Although it is characterized by a longer duration than munition hit and explosion, it is much more suitable than seismic loading that has an even longer duration and causes much lower accelerations.

The shape of the seismic fragility curve of the AP1000 was adopted (similar to MCEER-08–0019, 2008, [25]). The PGA within the NPP of the reference scenario is 12 g for the GBU-28 explosion at 3 m standoff from the NPP shielding wall (as described in Paragraph 4 above). The Standard deviation (βc) was assumed to be similar to the values referred to in the AP1000 design manual for seismic design. This assumption has to be verified in further research. Since considerable uncertainty is associated with the standard deviation of the PGA, sensitivity analyses were carried out to evaluate how sensitive the findings of the suggested model are and to assess the sensitivity of the overall probability of failure and the risk to the above parameters.

Further investigation has to be carried out to check these assumptions. Table 1 presents the lower and upper bounds of the probability of the basic events as well as of the RCS_F top event. Here, median capacity limits were best-matched to the equipment functions, as appears in Table 3 from NEI 07–13 (Revision 8P). The mean probabilities of failures of the critical components at the primary coolant cycle are found to be up to $5 \cdot 10^{-2,}$ and the subsequent mean probability of RCS_F event under the occurrence of the reference scenario is $8 \cdot 10^{-2}$. This probability of failure is for the occurrence of a single threat scenario event.

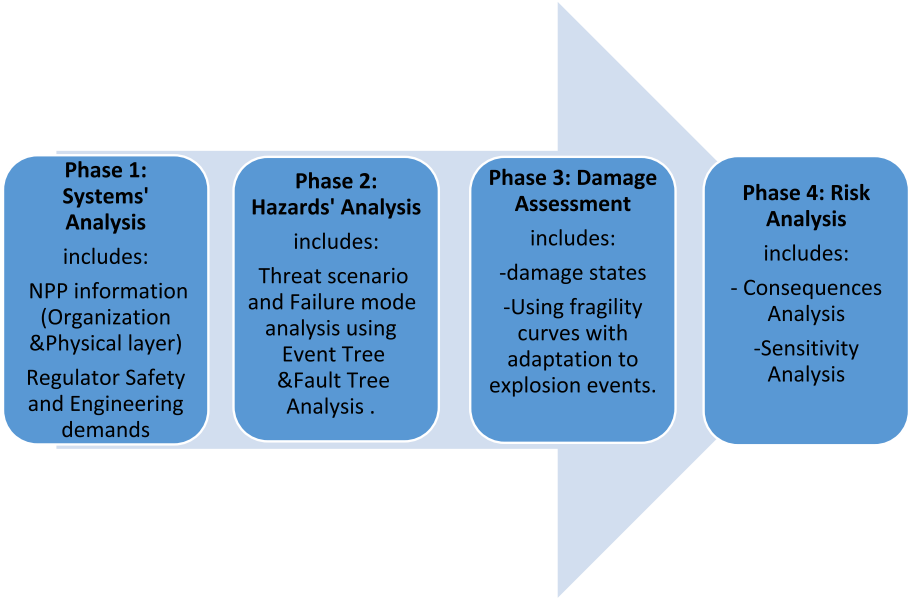

Fig. 22. PRA (Probabilistic Risk Assessment) Model Flowchart.

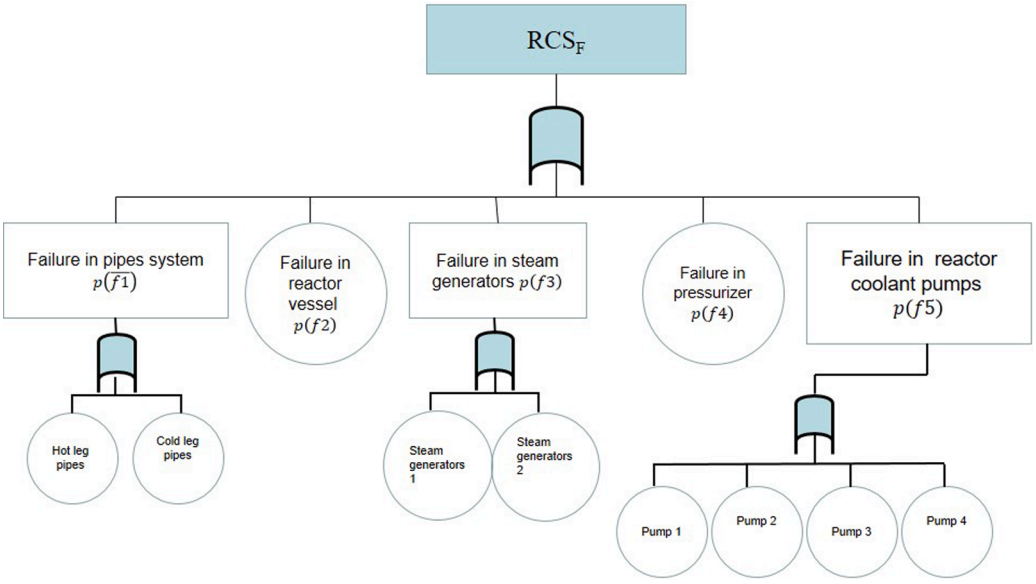

Fig. 23. Fault Tree Analysis of the Reactor Coolant System components that can lead to LOCA scenario in the AP1000 NPP.

Table 2
Mean, Upper and Lower bounds of annual = failure probabilities in Pressurizer, Cooling pumps and Valve and the derived bound for RCS_F in AP1000 caused by GBU-28 hit – a conservative approach.

Component	Median (g)	β_c	Lower limit (Probability of Failure)	Mean Probability of Failure	Upper limit (Probability of Failure)
Pipes system $p(f1)$	27	0.61	$2.25 \cdot 10^{-6}$	0.051	0.2561
Reactor vessel $p(f2)$	27	0.35	$3.54 \cdot 10^{-5}$	0.0027	0.1478
Steam generators $p(f3)$	27	0.33	$1.57 \cdot 10^{-5}$	0.0013	0.2651
Pressurizer $p(f4)$	27	0.31	$1.123 \cdot 10^{-6}$	0.0007	0.1375
Reactor coolant pumps $p(f5)$	27	0.51	$4.50 \cdot 10^{-6}$	0.0257	0.4466
RCS_F	–	–	$5.91 \cdot 10^{-5}$	0.08	0.777

Table 3
Mean, Upper and Lower bounds of annual failure probabilities in Pressurizer, Cooling pumps and Valve and the derived bound for RCS_F in AP1000 caused by GBU-28 hit according to moderated approach, with best available equipment data matching.

Component	Median (g)	β_c	Lower limit (Probability of Failure)	Mean Probability of Failure	Upper limit (Probability of Failure)
Pipes system $p(f1)$	27 (No data Assume Cat. A)	0.61	0.004	0.052	0.265
Reactor vessel $p(f2)$	108 (Tank data Cat. D)	0.35	$3.13 \cdot 10^{-15}$	$5.28 \cdot 10^{-12}$	$3.34 \cdot 10^{-9}$
Steam generators $p(f3)$	108 (Heat E. data Cat. D)	0.33	$1.10 \cdot 10^{-16}$	$2.78 \cdot 10^{-13}$	$2.64 \times \cdot 10^{-10}$
Pressurizer $p(f4)$	108 (Tank data Cat. D)	0.31	$2.05 \cdot 10^{-18}$	$8.21 \cdot 10^{-15}$	$1.23 \cdot 10^{-11}$
Reactor coolant pumps $p(f5)$	54 (Pump data Cat. B)	0.51	$8.28 \cdot 10^{-6}$	$4.72 \cdot 10^{-4}$	0.01
RCS_F	–	–	$4.30 \cdot 10^{-3}$	0.05	$2.73x10^{-1}$

6. Conclusion and discussion

A comprehensive introduction of the AP1000 nuclear power plant and its critical components was presented. It continues with the representation of the reference scenario, vulnerability analysis of the shielding structure wall, hydrodynamic simulations of the AP1000 response to blast loading, a risk assessment methodology, and a review of the essential mathematical tools.

The dynamic analyses and the simulations yield two major results:

- The AP1000 shielding wall might be breached due to GBU-28 hit from contact explosion up to 1 m standoff from the shielding wall.
- The internal systems might be damaged because of the in-structure shock caused by GBU-28 hit from contact explosion up to 3 m standoff from the shielding wall that may initiate LOCA.

The most important insights from the risk assessment procedures are detailed below.

- This research provides a deeper understanding of the limitations in using fragility curves for the analysis of expected failure modes due to nearby explosions. Current literature does not provide appropriate data for high explosive blasts. The difficulty lies in the fact that explosions have a unique feature of short duration and highly intense loading in comparison with the earthquake loading. Therefore, several adjustments must be considered in the risk analysis and assessment due to explosion events by using airplane crash data, which are more relevant. This leads to novelty and important insights into the current state of the art while examining the risks of NPP under explosion events.
- The analysis is focused on the main Reactor Coolant System components: hot and cold leg pipes, reactor coolant pumps, and the pressurizer safety nozzle. A failure in one of these components may lead to Large or Small LOCA.
- The findings reveal that the risk of Reactor Coolant System failure given the reference threat scenario of GBU-28 hit is non-negligible and may lead to LOCA event if the safety systems fail to respond. At the given scenario, the probabilities of failure of the critical components, e.g., pressurizer, cooling pumps, and valves are in the order of 0.05–0.08.
- The risk presented in this research is calculated following two approaches: conservative and moderate. The first one assumed a unified lower median fragility of all components in the failure mechanism. In contrast, the latter uses different fragilities for each component according to the NEI 07–13 (Revision 8P) that refer to an aircraft crash, which represents the median fragility limit of the NPP equipment.

The research model can be implemented for further development of AP1000, based on the findings of this rather limited research, and it is suggested that:

1. Owners of AP1000 NPP's in areas of conflict or potential terror perform blast simulations and risk assessment and analysis to ensure the NPP safety and the surrounding population and environment.
2. To investigate the use of appropriate mitigation devices for contact and near-miss blasts such as exterior protective layers and mitigation devices for the critical components.

The pipes of the reactor's primary coolant system are found to be the most vulnerable component among all other critical components of the AP1000 NPP coolant system. The scenario of a pipe rupture is the most probable one by several orders of magnitude. The RCS_F value is practically determined, to a large extent, by the mean probability of failure of the pipes system, in both the conservative and the moderate approaches.

Two main critical assumptions underlay this research. First, the median fragility values were taken from an aircraft crash that represents the median fragility conservative limit with respect to the explosion. This is due to the shorter duration of the dynamic load. The aircraft crash data is much more suitable than seismic data, which represents even longer dynamic load duration. Second, the standard deviation (β_c) was assumed to be similar to the values referred to in the AP1000 design manual for seismic design. This assumption was not verified in the present research and requires further study.

There is an inherent limitation in this kind of research. This limitation originates from the fact that experimental data and typical fragility curves of critical components in the AP1000 NPP under explosive blast load are not available. This data can only be obtained by large-scale experiments or highly complicated numerical simulations. This research intends to introduce the preliminary principle directions and methodologies for risk assessment, management, and coping actions for NPP hit by explosive warheads.

Funding

This research was supported by the Ministry of Energy of the State of Israel, Grant No. 214–11-011.

The authors are grateful to the Ministry of Energy officers for leadership and funding.

Declaration of Competing Interest

The authors declare that they have no known competing financial interests or personal relationships that could have appeared to influence the work reported in this paper.

References

[1] B.M. Abou-Zeid, W.W. El-Dakhakhni, A.G. Razaqpur, S. Foo, Performance of Unreinforced Masonry Walls Retrofitted with Externally Anchored Steel Studs under Blast Loading, J. Perform. Constr. Facil 25 (5) (2011) 441–453.

[2] A. Armenta-Molina, A. Villanueva-García, G. Soto-Mendoza, S. Pérez-Montejo, P. Ruiz-López, J.A. Beltrán-Fernández, L.H. Hernández-Gómez, G.M. Urriolagoitia-Calderón, Structural Vibrations in a Building of a Nuclear Power Plant Caused by an Underground Blasting Engineering Design Applications III, Adv. Struct. Mater. 124 (2020) 81–90.

[3] ASCE., 2010. "Design of Blast-Resistant Buildings in Petrochemical Facilities." ASCE Publications, 2010, Virginia, USA.

[4] J.M. Biggs, Introduction to Structural Dynamics, McGraw-Hill College, N.Y, U.S.A, 1964.

[5] Bluvband, Z., Polak, R., and Grabov, P., 2005. "Bouncing failure analysis (BFA): the unified FTA-FMEA methodology." Annual Reliability and Maintainability Symposium, 2005. Proceedings. IEEE, Alexandria, VA, USA, 463-467.

[6] I. Brandys, D. Ornai, Y. Ronen, Integrated Blast Resistance Model of Nuclear Power Plant Auxiliary Facilities, J. Nucl. Eng. Radiat. Sci. 3 (3) (2017) 030903–30908.

[7] M. Čepin, L. Cizelj, M. Leskovar, B. Mavko, Vulnerability Analysis of a Nuclear Power Plant Considering Detonations of Explosive Devices, J. Nucl. Sci. Technol. 43 (10) (2006) 1258–1269.

[8] L. Chadad, O. Vilnay, R. Levy, D. Ornai, The feasibility of passive controlled structural mechanism method to the design of structures, Eng. Struct. 155 (2018) 167–177.

[9] J. Choi, S. Choi, J.J. Kim, K. Hong, Evaluation of blast resistance and failure behavior of prestressed concrete under blast loading, Constr. Build. Mater. 173 (2018) 550–572.

[10] M.C. Constantinou, T.T. Soong, G.F. Dargush, Passive energy dissipation systems for structural design and retrofit, Multidisciplinary Center for Earthquake Engineering Research (MCEER), Buffalo, N.Y, 1998.

[11] Crowley, A. B., 2006. "The effect of munition casings on reducing blast overpressures." Insensitive Munitions Energ. Mater Tech. Symp. (IMEMTS), Bristol, United Kingdom.

[12] Department of Defense., 2008. "USA, Structures to Resist the Effects of Accidental Explosions (UFC 3-340-02) including 2014 revision".

[13] J.L. Drake, L.A. Twisdale, R.A. Frank, W.C. Dass, M.A. Rochefort, R.E. Walker, J. R. Britt, C.E. Murphy, T.R. Slawson, R.H. Sues, Protective Construction Design Manual: Air blast Effects, Air Force Engineering & Services Center, Tyndall Air Force Base, FL, 1989.

[14] D.O. Dusenberry, Handbook for Blast Resistant Design of Buildings, John Wiley & Sons, Hoboken, New Jersey, 2010.

[15] B.C. Ezell, S.P. Bennett, D. Von Winterfeldt, J. Sokolowski, A.J. Collins, Probabilistic Risk Analysis and Terrorism Risk, Risk Anal. 30 (4) (2010) 575–589.

[16] M.H. Faber, M.G. Stewart, Risk assessment for civil engineering facilities: critical overview and discussion, Reliab. Eng. Syst. Saf. 80 (2) (2003) 173–184.

[17] H.V. GangaRao, N. Taly, P.V. Vijay, Reinforced Concrete Design with FRP Composites, CRC Press, Boca Raton, FL, 2006.

[18] Georgakopoulos, P., and Koklanos, P., 2012. "Design, Detailing, and Architectural Impacts of Fiber Reinforced Polymers (FRP) and Geotextile Fabrics in the Blast Mitigation of Unreinforced Masonry Walls in Historic Buildings." Structures Congress 2012, ASCE, 358-369.

[19] A. Goel, R.J. Graves, Using failure mode effect analysis to increase electronic systems reliability, in: 2007 30th International Spring Seminar on Electronics Technology (ISSE), 2007, pp. 128–133.

[20] A. Gofuku, S. Koide, N. Shimada, Fault tree analysis and failure mode effects analysis based on multi-level flow modeling and causality estimation, in: 2006 SICE-ICASE International Joint Conference, 2006, pp. 497–500.

[21] S. Guruprasad, A. Mukherjee, Layered sacrificial claddings under blast loading Part I—analytical studies, Int. J. Impact Eng. 24 (9) (2000) 957–973.

[22] J. Ha, N. Yi, J. Choi, J.J. Kim, Experimental study on hybrid CFRP-PU strengthening effect on RC panels under blast loading, Compos. Struct. 93 (8) (2011) 2070–2082.

[23] H. Hader, Effects of Bare and cased Explosive Charges on Reinforced Concrete Walls, The Interaction of Non-Nuclear Munitions with Structures, Eaglin Air Force Base, 1985, pp. 221–226.

[24] P.J. Heffernan, R.G. Wight, M. Erki, Research on the Use of FRP for critical load-bearing infrastructure in conflict zones, J. Compos. Constr. 15 (2) (2010) 136–145.

[25] Huang, Y., Whittaker, A. S., and Luco, N., 2008. "Performance assessment of conventional and base-isolated nuclear power plants for earthquake and blast loadings." MCEER University at Buffalo, State University of New York, University at Buffalo, State University of New York.

[26] Y. Huang, A.S. Whittaker, Vulnerability Assessment of Conventional and Base-Isolated Nuclear Power Plants to Blast Loadings, Int. J. Protect. Struct. 4 (4) (2013) 545–563.

[27] M.D. Hutchinson, Effect of casing yield stress on bomb blast impulse, EPJ Web of Conferences 26 (2012) 4001.

[28] IAEA, 2003. "IAEA Safety Standards Series - Safety Guide NS-G-1.5." External Events Excluding Earthquakes in the Design of Nuclear Power Plants, International Atomic Energy Agency, Safety Guide No.

[29] S. Jeon, B. Jin, Improvement of impact-resistance of a nuclear containment building using fiber reinforced concrete, Nucl. Eng. Des. 304 (2016) 139–150.

[30] P. Jiang, Y.Y. Haimes, Risk Management for Leontief-Based Interdependent Systems, Risk Anal. 24 (5) (2004) 1215–1229.

[31] J.H. Kim, I.K. Choi, J.H. Park, Uncertainty analysis of system fragility for seismic safety evaluation of NPP, Nucl. Eng. Des. 241 (7) (2011) 2570–2579.

[32] K.W. King, J.H. Wawclawczyk, C. Ozbey, Retrofit strategies to protect structures from blast loading, Can. J. Civ. Eng. 36 (8) (2009) 1345–1355.

[33] T. Krauthammer, Reactive Protection for Hardened Facilities, Air Force Engineering and Services Center, Tyndall AFB, Florida, 1989.

[34] MSC Software Corporation., 2008. "MSC/Dytran Code.".

[35] C. Naito, R. Dinan, B. Bewick, Use of Precast Concrete Walls for Blast Protection of Steel Stud Construction, J. Perform. Constr. Facil 25 (5) (2011) 454–463.

[36] Nuclear Energy Institute, 2011. "Methodology for Performing Aircraft Impact Assessments for New Plant Designs." Nuclear Energy Institute (NEI), 2001 Walnut Creek, Ca.

[37] Oliveira, R. S. d., Cardoso, T., Prates, C. L. M., Riera, J. D., Iturrioz, I., and Kosteski, L. E., 2014. "Considerations concerning the analysis of NPP structures subjected to blast loading." Nuclear Engineering and Design, 269 171-176.

[38] S. Palanivelu, W. Van Paepegem, J. Degrieck, B. Reymen, J. Ndambi, J. Vantomme, D. Kakogiannis, J. Wastiels, D. Van Hemelrijck, Close-range blast loading on empty recyclable metal beverage cans for use in sacrificial cladding structure, Eng. Struct. 33 (6) (2011) 1966–1987.

[39] A.K. Pandey, D.K. Paul, Damage evaluation of a reinforced concrete containment shell subjected to blast loading, Curr. Sci. 97 (3) (2009) 336–341.

[40] C.A. Pinto, J.H. Lambert, Risk of Extreme Events in the Configuration of Priority Systems, Reliab. Eng. Syst. Saf. 76 (2002) 265–271.

[41] S.N. Raman, T. Ngo, P. Mendis, A review on the use of polymeric coatings for retrofitting of structural elements against blast effects, Electronic J. Struct. Eng. 11 (2011) 69–80.

[42] A. Schenker, I. Anteby, E. Nizri, B. Ostraich, Y. Kivity, O. Sadot, O. Haham, R. Michaelis, E. Gal, G. Ben-Dor, Foam-Protected Reinforced Concrete Structures under Impact: Experimental and Numerical Studies, J. Struct. Eng. 131 (8) (2005) 1233–1242.

[43] I.M. Shohet, D. Ornai, R. Levy, O. Vilnay, G. Ben-Dor, E. Gilad, E. Gal, B. Tavron, Y. Kivity, S.M. Elkabets, A methodology of risk assessment, management and coping actions for nuclear power plant hit by high-explosive warheads, Ben-Gurion University of the Negev, Beer Sheva, 2018.

[44] Sinnamon, R. M., and Andrews, J. D., 1996. "Fault tree analysis and binary decision diagrams." Proceedings of 1996 Annual Reliability and Maintainability Symposium, IEEE, Las Vegas, NV, USA, 215-222.

[45] M.M. Swisdak Jr, Simplified Kingery Airblast Calculations, NAVAL SURFACE WARFARE CENTER INDIAN HEAD DIV MD, Silver Spring, MD, 1994.

[46] M. Tariverdi, H. Fotouhi, S. Moryadee, E. Miller-Hooks, Health care system disaster-resilience optimization given its reliance on interdependent critical lifelines, J Infrastruct Syst 25 (1) (2019) 04018044.

[47] M.D. Theobald, G.N. Nurick, Experimental and numerical analysis of tube-core claddings under blast loads, Int. J. Impact Eng. 37 (3) (2010) 333–348.

[48] USAF, 1998. Procurement Program of Ammunition, Budget estimates for the fiscal year 1999, Unclassified, Feb. 1998.

[49] U.S. Nuclear Regulatory Commission, 2011. "Final Safety Evaluation Report, Related to Certification of the AP1000 Standard Plant Design, NUREG-1793 Volume 3 Supplement 2, Docket No. 52-006, ML11292A113." Washington, DC.

[50] U.S. Nuclear Regulatory Commission, 2017. "50.46 Acceptance criteria for emergency core cooling systems for light-water nuclear power reactors." https://www.nrc.gov/reading-rm/doc-collections/cfr/part050/part050-0046.html (Dec. 30, 2018).

[51] U.S. Nuclear Regulatory Commission (2011). https://www.nrc.gov/docs/ML1117/ML11171A500.html.

[52] United States Nuclear Regulatory Commission. (2011). "Westinghouse AP1000 Design Control Document Rev.19, 2011.".

[53] W.E. Vesely, F.F. Goldberg, N.H. Roberts, D.F. Haasl, Fault tree handbook, Nuclear Regulatory Commission Washington DC, Washington, DC, 1981.

[54] N. Vodopivec, E. Miller-Hooks, Transit system resilience: Quantifying the impacts of disruptions on diverse populations, Reliab. Eng. Syst. Saf. 191 (2019), 106561.

[55] M.G. Whitney, K.H. Spivey, Quantity Distance Requirements for Earth-Bermed Aircraft Shelters, BAKER (WILFRED) ENGINEERING, SAN ANTONIO TX, 1993.

[56] C. Wu, L. Huang, D.J. Oehlers, Blast testing of aluminum foam–protected reinforced concrete slabs, J. Perform. Constr. Facil 25 (5) (2010) 464–474.

[57] C. Zhao, X. Lu, Q. Wang, A. Gautam, J. Wang, Y.L. Mo, Experimental and numerical investigation of steel-concrete (SC) slabs under contact blast loading, Eng. Struct. 196 (2019), 109337.

[58] C. Zhao, Q. Wang, X. Lu, J. Wang, Numerical study on dynamic behaviors of NRC slabs in containment dome subjected to close-in blast loading, Thin-Walled Struct. 135 (2019) 269–284.